Computationally Efficient Time-Recursive IAA-Based Blood Velocity Estimation

Jakobsson, Andreas; Glentis, George; Gudmundson, Erik

Computationally Efficient Time-Recursive
IAA-Based Blood Velocity Estimation

A. JAKOBSSON, G. O. GLENTIS, AND E. GUDMUNDSON

Lund 2012

Mathematical Statistics
Centre for Mathematical Sciences
Lund University

Computationally Efficient Time-Recursive IAA-Based Blood Velocity Estimation

A. Jakobsson*, *Senior Member, IEEE*, G. O. Glentis†, *Member, IEEE*, and E. Gudmundson*

Abstract— High-resolution spectral Doppler is an important and powerful non-invasive tool for estimation of velocities in blood vessels using medical ultrasound scanners. Such estimates are typically formed using an averaged periodogram technique, resulting in well-known limitations in the resulting spectral resolution. Recently, we have proposed techniques to instead form high-resolution data-adaptive estimates exploiting measurements along both depth and emission. The resulting estimates gives noticeably superior velocity estimates as compared to the standard technique, but suffers from a high computational complexity, making it interesting to formulate computationally efficient implementations of the estimators. In this work, by exploiting the rich structure of the iterative adaptive approach (IAA) based estimator, we examine how these estimates can be efficiently implemented in a time-recursive manner using both exact and approximate formulations of the method. The resulting algorithms are shown to reduce the necessary computational load with several orders of magnitude without noticeable loss of performance.

Index Terms— Blood velocity estimation, medical ultrasound, irregular sampling, spectral estimation, iterative adaptive approach (IAA), fast algorithms.

I. INTRODUCTION

MEDICAL ultrasound is a powerful and frequently used technique for non-invasive estimation of velocities in blood vessels, allowing the physician not only to get an image of the blood vessel, but also of the flow dynamics in it, allowing, for instance, for the diagnosing of carotid artery stenosis [1]. Typically, the velocity of the moving blood is estimated using repeated transmissions focused at a single location repeatedly, and then forming a signal that is sampled once per emission after a time selected to allow the backscattered signal to be received from the depth of interest. The resulting signal, often termed a slow-time signal, will then have a frequency that is proportional to the axial blood velocity, i.e., the velocity along the direction of interrogation, such that for a single blood scatterer, the measured frequency will be $f_p = 2vf_c/c$, where v is the blood velocity along the ultrasound direction, $c = 1540$ m/s is the speed of propagation, and f_c the emitted ultrasound (center) frequency (typically 3-10 MHz). The velocity is then found by estimating the spectral content of the slow-time signal, which is generally being done using a Welch's periodogram estimate. The resulting estimate suffers from the well known limitation of this technique, necessitating that a large number of transmissions (about 100) are used to form the estimate, thereby reducing the temporal resolution of the estimate, making it difficult to see the details in the rapid acceleration phases of the cardiac cycle. Interleaved with the velocity transmissions are also transmissions used to form the B-mode image, allowing the

*A. Jakobsson and E. Gudmundson are with the Dept. of Mathematical Statistics, Lund University, P.O. Box 118, SE-221 00 Lund, Sweden, email: {aj,erikg}@maths.lth.se. E. Gudmundson is also with the Signal Processing Lab, ACCESS Linnaeus Center, KTH - Royal Institute of Technology, SE-100 44 Stockholm, Sweden.

†G. O. Glentis is with the Department of Science and Technology of Telecommunications, University of Peloponnese, Tripolis, 22100 Greece, email: gglentis@uop.gr.

physician to visualize and find the blood vessel, and to position the velocity estimation at the point of interest. These emissions are often interleaved so that every second transmission is a B-mode acquisition, thereby reducing the velocity range by a factor of two [2]. For vessels with high flow dynamics, one may instead choose to use blocks of emissions to acquire the B-mode image, but this will then result in holes in the blood velocity spectrogram [3]. To address this problem, different parametric and data-adaptive non-parametric spectral estimation techniques have been developed in the literature (see, e.g. [4]–[11]). In [10], the authors introduced data-adaptive Capon- and APES-based blood velocity spectral estimation techniques exploiting the information along both emissions and depth. These techniques were found to offer substantial improvements over the traditionally used Welch's method, results which have later also been confirmed in thorough *in vivo* studies [12], [13]. To allow for blocks of B-mode emissions, the technique was later also extended to periodically gapped data in [14]. Exploiting recent work in MIMO radar and RF spectroscopy [15]–[18], we presented an Iterative Adaptive Approach (IAA) algorithm that was found to improve on these results further still [19], although this gain was achieved at a noticeably higher computational cost. In [20], we presented a computationally efficient and exact block implementation of the so-called Blood Iterative Adaptive Approach (BIAA) algorithm using suitable Gohberg-Semencul (GS) representations to exploit the rich structure of the algorithm, dramatically reducing the required computational burden of the algorithm. Regrettably, although showing excellent performance, the overall complexity of the BIAA algorithm is still relatively high. In this work, we are therefore examining the possibility to formulate time-recursive exact and approximate implementations of the algorithm. As the blood velocity signal exhibits a periodically gapped structure, we exploit the exact block BIAA algorithm discussed in [19], [20] in forming the time-updating, thereby also generalizing the *sample-based* time-recursive formulation of the general IAA algorithm presented in [21] to a block form. Furthermore, generalizing the approximate Quasi-Newton (block) algorithm introduced in [22], we propose an approximate block-recursive updating algorithm which offers further notable computational savings without more than a marginal loss of performance. In the following section, we present an overview of the data model and an approximate formulation of the BIAA algorithm proposed in [19], formulating the problem of interest. Then, in Section III, we review the resulting reformulation of the exact fast BIAA (F-BIAA) implementation proposed in [20] and introduce the notation and structure for the derivation of the block-recursive exact and approximate algorithms proposed in Sections IV and V. In Section VI, we examine the performance and computational reductions offered by the discussed algorithms. Finally, Section VII contains our conclusions.

II. DATA MODEL AND THE BIAA METHOD

The ultrasound signal is measured by applying ultrasound pulses in a series of emissions. These ultrasound pulses will reflect on the various scatterers along the direction of interrogation, causing

the backscattered signal to be a function of the scatterers at the depths corresponding to the round-time of the propagation. The phase difference resulting from reflections at a given depth for different emissions will yield a signal with frequency that is related to the velocity of the scatterer. The thus obtained noise-free slow-time data acquired along emissions by the spectral Doppler at depth k, corresponding to emission n, for blood scatterers with (axial) velocity v, is commonly modeled as [2], [10]

$$\tilde{x}_k(n) = \alpha_v^{(k)} e^{j\phi_c k + j\psi_v n}, \tag{1}$$

where $\alpha_v^{(k)}$ is the (complex-valued) amplitude of the sinusoidal signal at frequency ψ_v, at depth k, which is directly related to the (axial) blood velocity, v, as

$$\psi_v = -\frac{2\omega_c}{cf_{prf}}v = -\frac{2v}{c}\omega_c T_{prf}, \tag{2}$$

where $\omega_c = 2\pi f_c$, f_{prf} is the pulse repetition frequency, and $T_{prf} = f_{prf}^{-1}$ is the time between pulse repetitions. Furthermore, ϕ_c is the demodulating frequency, relating the samples along each emission (the so-called fast-time), defined as $\phi_c = \omega_c/f_s$, where f_s is the sampling frequency. Combining the contributions from scatters for M considered velocities, one may write the measured, noise corrupted, signal as

$$x_k(n) = \sum_{m=1}^{M} \alpha_{v_m}^{(k)} e^{j\phi_c k + j\psi_{v_m} n} + w_k(n), \tag{3}$$

where $\{v_m\}_{m=1}^{M}$ denotes the m:th (axial) velocity, and $w_k(n)$ denotes a residual term consisting of all signals at velocities different from the M considered velocities as well as additive noise. From (2) and (3), it is clear that the spectral density of $x_k(n)$ with respect to ψ_{v_z} is equivalent to the blood velocity distribution at the examined location. The problem of estimating the blood velocity distribution can thus be seen to be equivalent to the estimation of $|\alpha_v|^2$ for all velocities of interest. Generally, the blood flow profile will be rather smooth along depth, implying that $\alpha_v^{(k)}$, over the depths $k = k_1, \ldots, k_K$, will be almost constant as long as the fast-time range is limited to be within the emitted pulse length. Here, we will exploit this smoothness and average the measured signals for adjacent depths, while compensated for the modulation along depth, and form

$$y(n) = \frac{1}{K} \sum_{k=k_1}^{k_K} e^{-j\phi_c k} x_k(n), \tag{4}$$

thereby increasing the signal to noise ratio (SNR) of the processed signal. Assuming uniform pulse emissions for either velocity estimation or B-mode imaging, the slow-time measurements may be viewed as exhibiting a reoccurring block structure, such that each block consists of the pattern of velocity and B-mode transmissions, typically having the form

$$\boldsymbol{y}_{N_g}(p) = \left[\begin{array}{ccc} y(pN_s) & \cdots & y(pN_s + N_g - 1) \end{array}\right]^T, \tag{5}$$

where $N_s = N_g + N_m$ and N_g and N_m denote the number of velocity emissions (given samples) and the number of B-mode emissions, here simply treated as missing samples, respectively. For the traditional case with every second emission being B-mode acquisitions, $N_g = N_m = 1$, but more general sampling patterns can also be used [3], [19]. The measurements used for velocity estimation at time p is then formed as the concatenation of the N_b most recent sub-blocks, i.e.,

$$\boldsymbol{z}_N(p) = \left[\begin{array}{ccc} \boldsymbol{y}_{N_g}^T(p - N_b + 1) & \cdots & \boldsymbol{y}_{N_g}^T(p) \end{array}\right]^T, \tag{6}$$

with the last sub-block being the most current measurements, and where $N = N_b N_g$ denotes the total number of available measurements in the observation window. Clearly, N will be limited

by the stationarity of the examined blood velocity signal, bounding how many emissions that may be used to form the resulting blood velocity spectral estimate. To improve the efficiency of the proposed implementations, we will initially exploit this block structure in measurements, and will then proceed to derive time-recursive formulations that exploit the already computed blood velocity estimate at time p to form the estimate at time $p + 1$. Let

$$\boldsymbol{a}_{\ell_1, \ell_2} = \left[\begin{array}{cccc} 1 & e^{j\psi_{v_m}\ell_1} & \cdots & e^{j\psi_{v_m}\ell_1(\ell_2-1)} \end{array}\right]^T \tag{7}$$

and form the gapped block Fourier vector, taking into account the missing samples, as

$$\bar{\boldsymbol{f}}_{\psi_{v_m}} = \boldsymbol{a}_{N_s, N_b} \otimes \boldsymbol{a}_{1, N_g}, \tag{8}$$

where $\otimes$ denotes the Kronecker product. The BIAA$_2$ algorithm is then formed, using the measurements up to time p, by iteratively estimating

$$\hat{\alpha}_{p, v_m} = \frac{\bar{\boldsymbol{f}}_{\psi_{v_m}}^H \boldsymbol{R}_N^{-1}(p) \boldsymbol{z}_N(p)}{\bar{\boldsymbol{f}}_{\psi_{v_m}}^H \boldsymbol{R}_N^{-1}(p) \bar{\boldsymbol{f}}_{\psi_{v_m}}}, \tag{9}$$

$$\boldsymbol{R}_N(p) = \sum_{m=1}^{M} |\hat{\alpha}_{p, v_m}|^2 \bar{\boldsymbol{f}}_{\psi_{v_m}} \bar{\boldsymbol{f}}_{\psi_{v_m}}^H, \tag{10}$$

until practical convergence, with $(\cdot)^H$ denoting the conjugate transpose. It is worth noting that, different from to the original BIAA algorithm in [19], we are here including the noise estimate in the covariance matrix estimate $\boldsymbol{R}_N(p)$. This change, just as the averaging in (4), allows for an overall speed-up that only implies a marginal loss of performance. To stress the difference between the here presented approximate version and the original BIAA algorithm proposed in [19], the former is here denoted BIAA$_2$. The computational complexity of the brute force implementation of the BIAA$_2$ algorithm is $C^{BIAA_2} = m\left[2N^2M + MN + N^3\right]$, where m is the number of iterations required for the convergence of the IAA algorithm, with 10 to 15 iterations typically being enough [15], [16]. For notational simplicity, we will in the following omit the dependence of p when this is clear from the context.

III. THE BLOCK-WISE FAST BIAA$_2$ ALGORITHM

In [20], we proposed a computationally efficient implementation of the BIAA algorithm, which we here, for completeness, and to introduce the necessary notation and structure, briefly review and generalize. The algorithm exploits that the covariance matrix in (10) will have a Toeplitz-block-Toeplitz (TBT) structure of the form [20]

$$\boldsymbol{R}_N = \begin{bmatrix} \boldsymbol{R}(0) & \boldsymbol{R}^H(1) & \cdots & \boldsymbol{R}^H(N_b-1) \\ \boldsymbol{R}(1) & \boldsymbol{R}(0) & \cdots & \boldsymbol{R}^H(N_b-2) \\ \vdots & \vdots & \ddots & \vdots \\ \boldsymbol{R}(N_b-1) & \boldsymbol{R}(N_b-2) & \cdots & \boldsymbol{R}(0) \end{bmatrix} \tag{11}$$

where $\boldsymbol{R}(\ell)$ denote the $N_g \times N_g$ (Toeplitz) covariance matrix of the ℓ:th sub-block. The matrix $\boldsymbol{R}_N$ can be recovered from a circulant matrix of higher dimensions as

$$\boldsymbol{C}_M = \mathcal{S}_M \begin{bmatrix} \boldsymbol{R}_N & \times \\ \times & \times \end{bmatrix} \mathcal{S}_M^T, \tag{12}$$

where $\mathcal{S}_M$ is a suitably chosen permutation matrix, $\times$ denotes unspecified terms of no relevance, and

$$\boldsymbol{C}_M = \boldsymbol{W}^H \text{diag}\left[\begin{array}{ccc} |\alpha_{v_1}|^2 & \cdots & |\alpha_{v_M}|^2 \end{array}\right] \boldsymbol{W}, \tag{13}$$

where $\boldsymbol{W}$ denotes the Discrete Fourier Transform (DFT) matrix of size $M \times M$, and $\text{diag}(\mathbf{x})$ denotes the diagonal matrix formed with the vector $\mathbf{x}$ along the diagonal. The first column of the circulant

matrix C_K, denoted c_K, can be computed using the Inverse DFT (IDFT) as $c_M = W^H \alpha_M$, where

$$\alpha_M = \begin{bmatrix} |\alpha_{v_1}|^2 & \dots & |\alpha_{v_M}|^2 \end{bmatrix}^T. \qquad (14)$$

Then, the lower (block) order partitions of (10) may be formed as

$$R_N = \begin{bmatrix} R_{N-N_g} & R_{N-N_g,N_g}^b \\ R_{N-N_g,N_g}^{bH} & R(0) \end{bmatrix} \qquad (15)$$

$$= \begin{bmatrix} R(0) & R_{N-N_g,N_g}^{fH} \\ R_{N-N_g,N_g}^f & R_{N-N_g,N_g} \end{bmatrix} \qquad (16)$$

where R_{N-N_g} is a TBT matrix of dimensions $(N-N_g) \times (N-N_g)$, whereas R_{N-N_g,N_g}^f and R_{N-N_g,N_g}^b are the forward and backward (block) matrices of size $(N - N_g) \times N_g$. Define

$$A_{N,N_g} = \begin{bmatrix} I_{N_g} \\ -R_{N-N_g}^{-1} R_{N-N_g,N_g}^f \end{bmatrix} \qquad (17)$$

$$B_{N,N_g} = \begin{bmatrix} -R_{N-N_g}^{-1} R_{N-N_g,N_g}^b \\ I_{N_g} \end{bmatrix} \qquad (18)$$

and

$$a_{N_g}^f = R(0) - R_{N-N_g,N_g}^{fH} R_{N-N_g}^{-1} R_{N-N_g,N_g}^f \qquad (19)$$

$$a_{N_g}^b = R(0) - R_{N-N_g,N_g}^{bH} R_{N-N_g}^{-1} R_{N-N_g,N_g}^b. \qquad (20)$$

The forward and backward predictors defined in (17) and (18), as well as the associated prediction error powers, as defined in (19) and (20), can efficiently be computed using the celebrated Levinson-Whittle-Wiggins-Robinson (LWWR) algorithm [23] (see also, e.g., [24], [25]). For completeness and for use in the following, the basic steps of the LWWR algorithm are tabulated in Table I. With these steps, the variable D_N, defined as

$$R_N D_N \triangleq z_N, \qquad (21)$$

that appears in (9), may be estimated using the LWWR algorithm as detailed in Table II. The computational complexity for the estimation of (17)-(20), as well as (21) using the LWWR algorithm described in Tables I and II, is $C^{LWWR} = 1.5N_b^2 N_g^3 + 2N_b N_g^3 + N_b^2 N_g^2$, where the last term accounts for the complexity for solving (21) using the order recursive scheme of Table II. Furthermore, using the GS factorization of $\mathbf{R}_N^{-1}$ and the block structure of the frequency vector, one may efficiently form the coefficients of the trigonometric polynomial that appear in the denominator of (9) using the FFT (see [20] for further details). The computational complexity of the resulting F-BIAA$_2$ algorithm is given by $C^{F-BIAA_2} = m[(1.5N_g + 1)N^2 + 3\phi(M) + 5N_g \phi(2N_b, 2N_g)]$, where $\phi(2N_b, 2N_s)$ and $\phi(M)$ denote the cost of computing a 2-D FFT of size $2N_b \times 2N_g$ as well as a 1-D FFT of size M, respectively.

IV. THE QUASI-NEWTON F-BIAA$_2$ ALGORITHM

Extending the results formulated in [22], we now proceed to propose an approximate block-wise F-BIAA$_2$ algorithm, where the covariance matrix $R_N(p)$ is substituted by an approximate estimate, which results in a substantially more efficient implementation, without having more than a marginal effect in the accuracy of the estimated parameters. The proposed method is motivated by the Quasi-Newton (QN) algorithm formulated in [26], and approximate the resulting Toeplitz covariance matrix as being formed from a low-order autoregressive (AR) process. The method, which has subsequently been applied to both adaptive acoustic echo cancellation and channel equalization [27]–[30], provides an efficient and low complexity implementation scheme of approximate recursive least squares algorithms by imposing a low order AR approximation on the input signal of the adaptive algorithm. Let $0 \leq q \leq N_b$ be the order

TABLE I
THE LWWR ALGORITHM AT STEP m WHERE $N = (m+1)N_g$ AND $m = 1, 2 \dots N_b - 1$

$$\begin{aligned}
\beta_{N_g} &= \mathbf{B}_{mN_g,N_g}^H \mathbf{R}_{mN_g,N_g}^f \\
\mathbf{k}_{N_g}^f &= a_{N_g}^{-f} \beta_{N_g} \\
\mathbf{k}_{N_g}^b &= a_{N_g}^{-b} \beta_{N_g}^H \\
\mathbf{A}_{(m+1)N_g,N_g} &= \begin{bmatrix} \mathbf{A}_{mN_g,N_g} \\ \mathbf{0}_{N_g} \end{bmatrix} + \begin{bmatrix} \mathbf{0}_{N_g} \\ \mathbf{B}_{mN_g,N_g} \end{bmatrix} \mathbf{k}_{N_g}^f \\
\mathbf{B}_{(m+1)N_g,N_g} &= \begin{bmatrix} \mathbf{0}_{N_g} \\ \mathbf{B}_{mN_g,N_g} \end{bmatrix} + \begin{bmatrix} \mathbf{A}_{mN_g,N_g} \\ \mathbf{0}_{N_g} \end{bmatrix} \mathbf{k}_{N_g}^b \\
a_{N_g}^f &= a_{N_g}^f + \beta_{N_g} \mathbf{k}_{N_g}^f \\
a_{N_g}^b &= a_{N_g}^b + \beta_{N_g}^H \mathbf{k}_{N_g}^f
\end{aligned}$$

TABLE II
ESTIMATION OF D_N USING THE LWWR ALGORITHM

$$\begin{aligned}
\beta_{N_g}^d &= \mathbf{B}_{mN_g,N_g}^H \mathbf{z}_{(m+1)N_g} \\
\mathbf{k}_{N_g}^d &= a_{N_g}^{-b} \beta_{N_g}^d \\
\mathbf{D}_{(m+1)N_g} &= \begin{bmatrix} \mathbf{D}_{mN_g} \\ \mathbf{0}_{N_g \times 1} \end{bmatrix} + \mathbf{B}_{mN_g,N_g} \mathbf{k}_{K_g}^d
\end{aligned}$$

of the QN approximation. Clearly, when $q = N_b$, the QN approach will produce the same results as the ordinary method. Consider the covariance matrix of order q, i.e.,

$$R_{N_q} \triangleq R_{qN_g} \qquad (22)$$

where R_{N_q} is TBT matrix of size $N_q \times N_q$ and where $N_q \triangleq qN_g$. Suppose that the inverse $R_{N_q}^{-1}$ has been computed using, for example, the LWWR algorithm of Table I. Let $R_{N_q+N_g}$ be the increased order covariance matrix. Then, using (16) and the matrix inversion lemma for partitioned matrices [31], one obtains

$$R_{N_q+N_g}^{-1} = \begin{bmatrix} 0 & \mathbf{0}^T \\ \mathbf{0} & R_{N_q}^{-1} \end{bmatrix} + \mathbf{A}_{N_q+N_g,N_g} a_{N_g}^{-1} \mathbf{A}_{N_q+N_g,N_g}^H \qquad (23)$$

which, using (18) and (20), yields

$$A_{N_q+N_g,N_g} = \begin{bmatrix} I_{N_g} \\ -R_{N_q}^{-1} R_{N_q,N_g}^f \end{bmatrix} \qquad (24)$$

$$a_{N_g}^f = R(0) - R_{N_q,N_g}^{fH} R_{N_q}^{-1} R_{N_q,N_g}^f. \qquad (25)$$

Recall that $A_{N_q+N_g,N_g}$ can be recursively updated using the LWWR algorithm of Table I as

$$\beta_{N_g} = \mathbf{B}_{N_q,N_g}^H \mathbf{R}_{N_q,N_g}^f \qquad (26)$$

$$\mathbf{k}_{N_g}^f = a_{N_g}^{-f} \beta_{N_g} \qquad (27)$$

$$A_{N_q+N_g,N_g} = \begin{bmatrix} \mathbf{A}_{N_q,N_g} \\ \mathbf{0}_{N_g} \end{bmatrix} + \begin{bmatrix} \mathbf{0}_{N_g} \\ \mathbf{B}_{N_q,N_g} \end{bmatrix} \mathbf{k}_{K_g}^f. \qquad (28)$$

Adopting the methodology presented in [26]–[28], the matrix R_{N_q} of dimensions $N_q \times N_q$ is extrapolated to an increased order matrix $\mathbf{Q}_{N_q+N_g}$ of dimensions $(N_q + N_g) \times (N_q + N_g)$, imposing the condition that

$$A_{N_q+N_g,N_g} = \begin{bmatrix} \mathbf{A}_{N_q,N_g} \\ \mathbf{0}_{N_g} \end{bmatrix} \qquad (29)$$
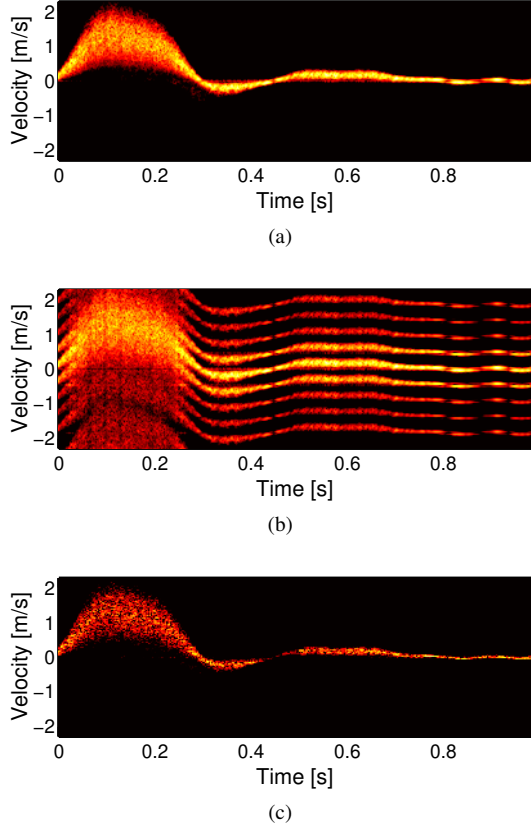
(a)

(b)

(c)

Fig. 1. (a) Reference spectrogram, created using Welch's method with all 130 emissions, as well as (b) the Welch's estimate and (c) the F-BIAA$_2$ spectrogram for data consisting of 13 blocks with emission pattern [1 1 1 1 1 1 0 0 0 0], with 33 samples along depth.

(a)

(b)

Fig. 2. (a) The BR-F-BIAA$_2$ and (b) BR-QN-F-BIAA$_2$ spectrograms, for data consisting of 13 blocks with emission pattern [1 1 1 1 1 1 0 0 0 0], with 33 samples along depth.

QN-F-BIAA$_2$ algorithm, is formed by iterating

$$\hat{\alpha}_{p,v_m} = \frac{\bar{\boldsymbol{f}}_{\psi_{v_m}}^H \mathbf{Q}_N^{-1}(p) \boldsymbol{z}_N(p)}{\bar{\boldsymbol{f}}_{\psi_{v_m}}^H \mathbf{Q}_N^{-1}(p) \bar{\boldsymbol{f}}_{\psi_{v_m}}} \qquad (32)$$

$$\boldsymbol{R}_{N_q}(p) = \sum_{m=1}^M |\hat{\alpha}_{p,v_m}|^2 \bar{\mathbf{f}}_{\psi_{v_m}} \bar{\mathbf{f}}_{\psi_{v_m}}^H \qquad (33)$$

$$\mathbf{Q}_N^{-1}(p) = \begin{bmatrix} \mathbf{0} & \mathbf{0}^T \\ \mathbf{0} & \mathbf{R}_{N_q}^{-1}(p) \end{bmatrix} + \mathbf{A}_{N,N-N_q}^Q \mathbf{A}_{N,N-N_q}^{QH}. \qquad (34)$$

The computational complexity of the resulting algorithm is given approximately by $C^{QN-F-BIAA_2} = m[(1.5q^2 + q)N_g^3 + 3\phi(M) + 5N_g\phi(2q, 2N_g)]$.

V. THE BLOCK RECURSIVE F-BIAA$_2$ ALGORITHM

Both the F-BIAA$_2$ and the QN-F-BIAA$_2$ algorithms may be computed in a block-recursive (BR) manner as new measurements become available. The algorithm may be simplified further by allowing for an approximate solution, noting that, upon convergence, the covariance matrix estimated at time p, i.e., $\boldsymbol{R}_N(p)$, can be used for the initialization of the covariance matrix at the successive time $p+1$, i.e., $\boldsymbol{R}_N(p+1)$, indicating that an approximate solution can be found by setting $m = 1$. Instead of iteratively solving (9) and (10) each time a new data block is available, a time varying updating scheme is applied as

$$\hat{\alpha}_{p,v_m} = \frac{\bar{\boldsymbol{f}}_{\psi_{v_m}}^H \boldsymbol{R}_N^{-1}(p) \boldsymbol{z}_N(p)}{\bar{\boldsymbol{f}}_{\psi_{v_m}}^H \boldsymbol{R}_N^{-1}(p) \bar{\boldsymbol{f}}_{\psi_{v_m}}} \qquad (35)$$

$$\boldsymbol{R}_N(p+1) = \sum_{m=1}^M |\hat{\alpha}_{p,v_m}|^2 \bar{\boldsymbol{f}}_{\psi_{v_m}} \bar{\boldsymbol{f}}_{\psi_{v_m}}^H, \qquad (36)$$

where the iterative updating of the spectral estimate sought and the time updating of the covariance matrix are both interleaved in a simplified two steps procedure. The resulting approximation does not induce any substantial loss in performance. Similar arguments apply to the block recursive implementation of the QN-F-BIAA$_2$ algorithm. We term the resulting approximate estimates the BR-F-BIAA$_2$ and BR-QN-F-BIAA$_2$ algorithms, respectively, noting that their computational complexity will be m times lower compared to the corresponding batch processing algorithms, where m denotes the number

or, equivalently, by setting $\boldsymbol{\beta}_{N_g} = \mathbf{0}$. Iterating this procedure up to N_b, one obtains the QN approximation of $\mathbf{R_N}$ as

$$\mathbf{Q}_N^{-1} = \begin{bmatrix} \mathbf{0} & \mathbf{0}^T \\ \mathbf{0} & \mathbf{R}_{N_q}^{-1} \end{bmatrix} + \mathbf{A}_{N,N-N_g N_q}^Q \mathbf{A}_{N,N-N_g N_q}^{QH} \qquad (30)$$

where

$$\mathbf{A}_{N,N-N_g N_q}^Q \triangleq \begin{bmatrix} \mathbf{A}_{N_q,N_g} & 0 & \cdots & 0 \\ 0 & \mathbf{A}_{N_q,N_g} & \ddots & \vdots \\ \vdots & 0 & \ddots & \vdots \\ \vdots & \vdots & \ddots & 0 \\ \vdots & \vdots & \ddots & \mathbf{A}_{N_q,N_g} \\ 0 & 0 & \ddots & 0 \end{bmatrix} \qquad (31)$$

is a $N \times (N - N_g N_q)$ block Toeplitz matrix with matrix entries of size $N_g \times N_g$. Thus, (31) results from an incomplete LWWR algorithm where, by construction, the forward and backward matrix valued reflection coefficient are set equal to zero, for $\ell = q+1, q+2, \ldots, N_b$. Using the results presented above, an approximate F-BIAA$_2$ algorithm can be derived by the direct use of the matrix $\mathbf{Q}_N(p)$, as defined in (30), in place of $\boldsymbol{R}_N(p)$ that appears in (9). Since the inverse $\mathbf{Q}_N^{-1}$ is already available, no further computations are required for this purpose. Thus, the resulting approximate algorithm, termed the
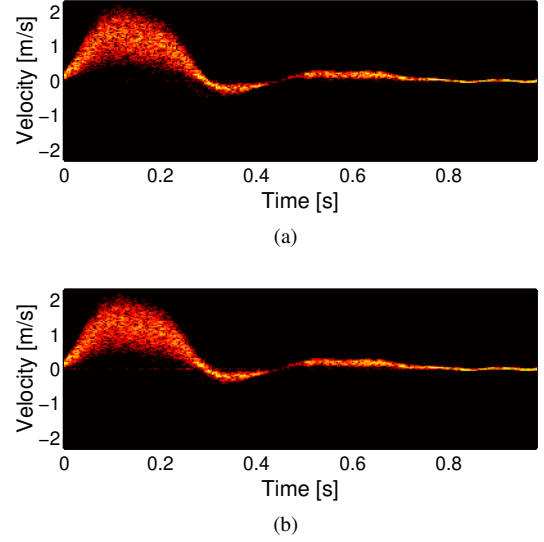
TABLE III
COMPUTATIONAL COMPLEXITY

Method	Batch	Block recursive
BIAA [19]	$8.2 \cdot 10^7$	-
F-BIAA [20]	$4.3 \cdot 10^6$	-
$BIAA_2$	$6.7 \cdot 10^7$	-
$F\text{-}BIAA_2$	$9 \cdot 10^5$	$9 \cdot 10^4$
$QN\text{-}F\text{-}BIAA_2$	$2 \cdot 10^5$	$2 \cdot 10^4$

of iterations required for the convergence of the original scheme, i.e., (9) and (10). The computational gain offered by the proposed methods is illustrated in Table III, where the approximate number of complex valued computations required by various algorithms (for 130 emissions and for the spectral estimate updating period equal to 10 emissions) is presented for the batch as well as for the block time recursive case, using the parameters described in detail in Section VI. Here, the number of the IAA iterations that is used in the batch methods is $m = 10$.

VI. NUMERICAL RESULTS

In order to evaluate the performance of the proposed algorithms, we examine both simulated data generated using the Field II toolbox [32], [33], mimicking the blood flow through a femoral artery, and *in vivo* data from the carotid artery of a healthy volunteer. Each spectrogram was generated using 500 equally spaced grid points in the interval $\psi_{v_z} \in [-0.5, 0.5)$, with emission scheme [1 1 1 1 1 1 0 0 0 0], using 13 blocks for each spectrum. Here, the '1' denotes an emission aimed at estimating the blood velocity, whereas a '0' denotes an emission aimed at forming a B-mode image. This yields 130 emissions, of which $6 \times 13 = 78$ emission were considered available for blood velocity estimation. Each emission thus yields a vector measurement along depth. We initially examine the simulated flow data, emulating femoral artery flow data using the Womersley model [34] for pulsating flow. The specific parameters for the flow simulation can be found in [3]. For signals taken in regions close to the vessel wall, the stationary part of the backscattered signal can be very strong, and would, if not removed, easily obstruct the blood velocity signal. As customary, we here do so using mean subtraction. In Figure 1, the Welch and the $F\text{-}BIAA_2$ spectrogram[1] using only 60% of the emission data (thereby allowing for 40% of the emissions to be used for B-mode imaging) is plotted together with a reference spectrogram, created using all 130 emissions with Welch's method. As is clear from the figure, the Welch estimate will fail to produce a meaningful estimate for the reduced data set, whereas the BIAA estimate is quite close to the reference estimate obtained using Welch's method for the full data set[2]. As is clear from the figure, the $F\text{-}BIAA_2$ algorithm allows for a highly accurate blood flow spectrogram even when using significantly fewer emissions than the reference method. Figure 2 shows the block-recursive $BR\text{-}F\text{-}BIAA_2$ and $BR\text{-}QN\text{-}F\text{-}BIAA_2$ spectrograms for the same settings as for the $F\text{-}BIAA_2$ spectrogram in Figure 1(b), where the value of $q = 4$ has been adopted in the $BR\text{-}QN\text{-}F\text{-}BIAA_2$ algorithm (recall that $q \leq N_b$). As discussed above, these algorithms exploit the block structure of the signal when computing the consecutive spectrograms, yielding a computational load of only 2% and 0.5%, respectively, as compared to that of the F-BIAA algorithm for the examined example, without introducing more than a marginal degradation of the resulting spectrograms. These spectrograms were produced using $K = 33$

(a)

(b)
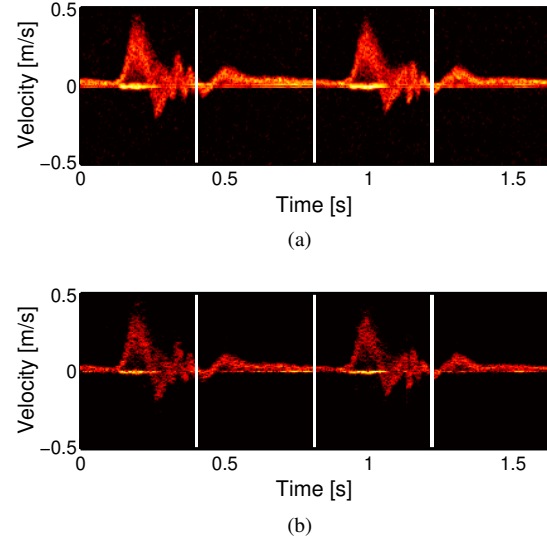
Fig. 3. (a) Reference spectrogram, created using Welch's method with all 130 emissions, and (b) $BR\text{-}QN\text{-}F\text{-}BIAA_2$ spectrogram, for data consisting of 13 blocks with emission pattern [1 1 1 1 1 1 0 0 0 0], with 40 samples along depth.

regularly spaced measurements along depths (fast-time samples) and using a dynamic range of 40 dB. To emphasize the performance of the BIAA algorithms, we also examine *in vivo* data, acquired using the experimental scanner RASMUS [35] and a B-K Medical 8804 7 MHz linear array transducer. This data set was previously used in [13], wherein further details on the setup may be found. As above, the stationary part of the signal was removed using mean subtraction. Here, all spectrograms were produced using $K = 40$ regularly spaced measurements along depths and using a dynamic range of 50 dB. Figure 3 shows the reference spectrogram created with Welch's method, using all 130 emissions per spectrum, and the $BR\text{-}QN\text{-}F\text{-}BIAA_2$ spectrogram using only 60% of the measurements. Again, we note that the proposed methods produce a clear spectrogram with significantly fewer emissions, allowing for interleaving the velocity measurements with B-mode image transmissions. The gaps in the spectrograms represent transmissions used for the necessary B-mode images during the data acquisition[3]. The $BR\text{-}QN\text{-}F\text{-}BIAA_2$ algorithm here requires just 0.5% of the computations required as compared to the F-BIAA algorithm. Finally, we examine the performance of the proposed implementation as compared to the exact method as well as the reference spectrogram. Table IV show the full width at half maximum (FWHM), given in 10^{-3} m/s, and the contrast (the ratio of the main lobe and the median of the side lobes), given in dB, for the in vivo data, at 0.91 s, which corresponds to end-diastole. The FWHM is a measure of spectral resolution and should be low, whereas the contrast should be high. As is clear from the table, the FWHM is notably lower and the contrast higher for the BIAA methods as compared to the reference Welch's spectrum, even though the reference used all 130 emissions whereas the BIAA methods only used 78 emissions. The contrast is about the same for the BIAA methods, whereas the FWHM is somewhat smaller for $F\text{-}BIAA_2$ as compared to the others. As noted above, Welch's method will fail to produce a meaningful estimate on the reduced data set.

---

[1]For this data set, the BIAA and $F\text{-}BIAA_2$ spectrogram estimates are visually indistinguishable.

[2]We note that the BIAA estimate will be almost indistinguishable from the spectrogram estimate if applied to the full data set [19].

[3]The gaps occur as the data set was obtained to evaluate the BAPES estimator [10] which requires regular emissions; thus, the B-mode transmissions for this data set differ from the ones assumed in the here examined example. We remark that if the B-mode emissions are done according to the assumed sampling pattern over emissions, no gaps would occur.

TABLE IV

COMPARISON OF FWHM AND CONTRAST FOR THE *in vivo* DATA

Method	FWHM (10^{-3} m/s)	Contrast (dB)
Reference spectrum	10.8	36
BIAA	5.1	40
F-BIAA$_2$	4.6	41
BR-F-BIAA$_2$	5.1	41
BR-QN-F-BIAA$_2$	5.2	42

VII. CONCLUSIONS

In this paper, we have presented an approximate reformulation of the recent BIAA algorithm, termed the BIAA$_2$ algorithm, allowing for a high-resolution data-adaptive blood velocity estimate that exploits measurements along both depth and emission. The algorithm allows for an arbitrary sampling along emissions, giving the operator freedom to vary the number of B-mode emissions as well as to, potentially, focus the velocity estimation to two separate locations in the blood vessel. A computationally efficient block implementation of the BIAA$_2$ algorithm has been proposed, exploiting the inherently low displacement rank of the involved matrices, as well as an approximate formulation allowing for notably lower computational complexity without more than a marginal loss of performance. Block-recursive formulations of these estimators have also been introduced, further substantially lowering the necessary computational complexity. The resulting techniques are found to reduce the necessary computational load with several orders of magnitude, while still allowing for the same high quality blood velocity estimates.

ACKNOWLEDGMENTS

REFERENCES

[1] R. W. J. Felix, B. Sigel, R. J. Gibson, J. Williams, and G. L. Popgy, "Pulsed Doppler ultrasound detection of flow disturbances in arteriosclerosis," *J. Clin. Ultrasound*, vol. 4, pp. 275–282, 1976.

[2] J. A. Jensen, *Estimation of Blood Velocities Using Ultrasound*, Cambridge University Press, New York, 1996.

[3] J. A. Jensen, "Spectral velocity estimation in ultrasound using sparse data sets," *Journal of Acoustical Society of America*, vol. 120, no. 1, pp. 211–220, July 2006.

[4] R. I. Kitney and D. P. Giddens, "Analysis of blood velocity waveforms by phase shift averaging and autoregressive spectral estimation," *J. Biomech. Eng.*, vol. 105, pp. 398–401, Nov. 1983.

[5] P. J. Vaitkus and R. S. C. Cobbold, "A comparative study and assessment of Doppler ultrasound spectral estimation techniques part I: Estimation methods," *Ultrasound in Medicine & Biology*, vol. 14, no. 8, pp. 661 – 672, 1988.

[6] P. J. Vaitkus, R. S. C. Cobbold, and K. W. Johnston, "A comparative study and assessment of Doppler ultrasound spectral estimation techniques, Part II: Methods and results," *Ultrasound Med. Biol.*, vol. 14, no. 8, pp. 673–688, 1988.

[7] F. S. Schlindwein and D. H. Evans, "A real time autoregressive spectrum analyzer for Doppler ultrasound signals," *Ultrasound Med. Biol.*, vol. 15, no. 3, pp. 263–272, 1989.

[8] M. E. Allam and J. F. Greenleaf, "Isomorphism between pulsed-wave Doppler ultrasound and direction-of-arrival estimation. I. Basic principles," *IEEE Transactions on Ultrasonics, Ferroelectrics, and Frequency Control*, vol. 43, no. 5, pp. 911–922, 1996.

[9] M. E. Allam, R. R. Kinnick, and J. F. Greenleaf, "Isomorphism between pulsed-wave Doppler ultrasound and direction-of-arrival estimation. II. Experimental results," *IEEE Transactions on Ultrasonics, Ferroelectrics, and Frequency Control*, vol. 43, no. 5, pp. 923–935, 1996.

[10] F. Gran, A. Jakobsson, and J. A. Jensen, "Adaptive Spectral Doppler Estimation," *IEEE Transactions on Ultrasonics, Ferroelectrics and Frequency Control*, vol. 56, no. 4, pp. 700–714, April 2009.

[11] S. Ricci, F. Guidi, and P. Tortoli, "Velocity profile detection through adaptive spectral estimators," in *2010 IEEE Ultrasonics Symposium (IUS)*, oct. 2010, pp. 57 –60.

[12] F. Gran, A. Jakobsson, J. Udesen, and J. A. Jensen, "Fast Spectral Velocity Estimation Using Adaptive Techniques: In-Vivo Results," in *IEEE Ultrasonics Symposium, 2007*, Oct. 2007, pp. 993–996.

[13] K. L. Hansen, F. Gran, M. M. Pedersen, I. K. Holfort, J. A. Jensen, and M. B. Nielsen, "In-vivo validation of fast spectral velocity estimation techniques," *Ultrasonics*, vol. 50, no. 1, pp. 52 – 59, 2010.

[14] P. Liu and Dong Liu, "Periodically gapped data spectral velocity estimation in medical ultrasound using spatial and temporal dimensions," in *ICASSP*, April 2009, pp. 437–440.

[15] T. Yardibi, J. Li, P. Stoica, M. Xue, and A. B. Baggeroer, "Source Localization and Sensing: A Nonparametric Iterative Approach Based on Weighted Least Squares," *IEEE Trans. on Aerospace and Electronic Systems*, vol. 46, no. 1, pp. 425–443, January 2010.

[16] P. Stoica, J. Li, and J. Ling, "Missing Data Recovery via a Nonparametric Iterative Adaptive Approach," *IEEE Signal Processing Letters*, vol. 16, no. 4, pp. 241–244, April 2009.

[17] E. Gudmundson, P. Stoica, J. Li, A. Jakobsson, M. D. Rowe, J. A. S. Smith, and J. Ling, "Spectral Estimation of Irregularly Sampled Exponentially Decaying Signals with Applications to RF Spectroscopy," *Journal of Magnetic Resonance*, vol. 203, no. 1, pp. 167–176, March 2010.

[18] X. Tan, W. Roberts, J. Li, and P. Stoica, "Sparse learning via iterative minimization with application to MIMO radar imaging," *IEEE Trans. Signal Processing*, vol. 59, no. 3, pp. 1088–1101, March 2011.

[19] E. Gudmundson, A. Jakobsson, J. A. Jensen, and P. Stoica, "Blood Velocity Estimation Using Ultrasound and Spectral Iterative Adaptive Approaches," *Signal Processing*, vol. 91, no. 5, pp. 1275–1283, May 2011.

[20] G.-O. Glentis and A. Jakobsson, "Efficient Implementation of Iterative Adaptive Approach Spectral Estimation Techniques," *IEEE Trans. Signal Processing*, vol. 59, no. 9, pp. 4154–4167, Sept. 2011.

[21] G.-O. Glentis and A. Jakobsson, "Time-Recursive IAA Spectral Estimation," *IEEE Signal Processing Letters*, vol. 18, no. 2, pp. 111–114, Feb. 2011.

[22] G.-O. Glentis and A. Jakobsson, "Superfast Approximative Implementation of the IAA Spectral Estimate," *IEEE Trans. Signal Processing*, vol. 60, no. 1, pp. 472–478, Jan. 2012.

[23] R. A. Wiggins and E. A. Robinson, "Recursive Solution of the Multichannel Filtering Problem," *J. Geophys. Res.*, vol. 70, pp. 1885–1891, April 1965.

[24] N. Kalouptsidis, G. Carayannis, and D. Manolakis, "Fast Algorithms for Block Toeplitz Matrices with Toeplitz Entries," *Signal Processing*, vol. 6, pp. 77–81, 1984.

[25] Jr. S. L. Marple, *Digital spectral analysis with applications*, Prentice Hall, Englewood Cliffs, NJ, 1987.

[26] G. V. Moustakides and S. Theodoridis, "Fast Newton Transversal Filters - A New Class of Adaptive Estimation Algorithms," *IEEE Trans. Signal Processing*, vol. 39, no. 10, pp. 2184–2193, Oct. 1991.

[27] B. Farhang-Boroujeny, "Fast LMS/Newton algorithms based on autoregressive modeling and their application to acoustic echo cancellation," *IEEE Trans. Signal Processing*, vol. 45, no. 8, pp. 1987–2000, August 1997.

[28] B. Farhang-Boroujeny and H. Rao, "Fast LMS/Newton algorithms for stereophonic acoustic echo cancellation," *IEEE Trans. Signal Processing*, vol. 57, no. 8, pp. 2919–2930, Aug. 2009.

[29] A. Gilloire, T. Petillon, and S. Theodoridis, "The fast Newton transversal filter: an efficient scheme for acoustic echo cancellation in mobile radio," *IEEE Trans. Signal Processing*, vol. 42, no. 3, pp. 509–518, March 1994.

[30] G. Moustakides, S. Theodoridis, and K. Berberidis, "A fast Newton multichannel algorithm for decision feedback equalization," *IEEE Trans. Signal Processing*, vol. 43, no. 1, pp. 327–331, Jan. 1995.

[31] P. Stoica and R. Moses, *Spectral Analysis of Signals*, Prentice Hall, Upper Saddle River, N.J., 2005.

[32] J. A. Jensen and N. B. Svendsen, "Calculation of pressure fields from arbitrarily shaped, apodized, and excited ultrasound transducers," *IEEE Trans. Ultrason., Ferroelec., Freq. Contr.*, vol. 39, pp. 262–267, 1992.

[33] J. A. Jensen, "Field: A Program for Simulating Ultrasound Systems," in *10th Nordic-Baltic Conference on Biomedical Imaging, Published in Medical & Biological Engineering & Computing*, 1996, vol. 34, Supplement 1, Part 1, p. 351353.

[34] J. R. Womersley, "Oscillatory motion of a viscous liquid in a thin-walled elastic tube. I: The linear approximation for long waves," *Phil. Mag.*, vol. 46, pp. 199–221, 1955.

[35] J. A. Jensen, O. Holm, L. J. Jerisen, H. Bendsen, S. I. Nikolov, B. G. Tomov, P. Munk, M. Hansen, K. Salomonsen, J. Hansen, K. Gormsen, H. M. Pedersen, and K. L. Gammelmark, "Ultrasound research scanner for real-time synthetic aperture data acquisition," *IEEE Transactions on Ultrasonics, Ferroelectrics and Frequency Control*, vol. 52, no. 5, pp. 881 –891, May 2005.